

# Control of convection by different buoyancy forces

Norman DAHLEY <sup>\*a</sup>, Birgit FUTTERER<sup>a</sup>, Christoph EGBERS<sup>a</sup>

<sup>a</sup>Brandenburg University of Technology Cottbus, Dept. Aerodynamics and Fluid Mechanics, Germany

\* Corresponding author: Tel.: ++49 (0)355 5123; Fax: ++49 (0)355 4545; Email: norman.dahley@tu-cottbus.de

**Abstract** Thermal convection in vertical concentric cylinders under the influence of different buoyancy force fields is the focus of the experimental project 'CiC' (Convection in Cylinders). The objectives are to investigate thermal convective flow in natural gravity with axial buoyancy and in micro-gravity environment of a parabolic flight with radial buoyancy, and additionally also the superposition of both buoyancy force fields. The radial buoyancy is forced by the dielectrophoretic effect due to applying a high-voltage potential  $V_{app}$  between the two cylinders. The experiment contains two separately fully automated experiment cells, which differ only in their radius ratio  $\eta = b/a$ . The convective flow is observed with tracer particles and laser light sheet illumination. For the case of natural convection, there exists a stable single convective cell over the whole Rayleigh number domain with  $Ra \sim \Delta T$  with increasing the temperature difference between the inner and outer cylindrical boundaries. For the case of a pure dielectrophoretic driven convection in micro-gravity environment, stratification effects are described with  $Ra_E \sim V_{app}$  with increasing the high voltage potential. The superposition of both buoyancy forces indicates the disturbance of the single convective cell and therewith the onset of instabilities at very low  $Ra$  for the smaller  $\eta$ . The presented results demonstrate that the dielectrophoretic effect can be used for flow control and enhancement of heat transfer applications in space as well as on Earth.

Keywords: flow control, convection, buoyancy-driven instabilities, dielectrophoretic effect, micro flow, micro gravity

## 1. Introduction

Research in microfluidics focuses on fluid dynamics at small scales. These small scales offer the possibility of setting up physical effects, which are more efficiently at those ranges. With regard to industrial applications, especially of electro-hydrodynamic forces, e.g. in heat exchangers, pumps and micro-dosing systems, cylindrical geometries come to the fore. The project 'Convection in a Cylinder' (CiC) studies heat transfer enhancement for the case of two concentric, vertically aligned cylinders at small scales. The annular cavity is defined by the radii  $a$  and  $b$ , resulting in a gap width of  $d = 5mm$ , and the length  $L = 100mm$ , which lead to an aspect ratio of  $\Gamma = L/d = 20$ . The cylindrical gap is filled with a dielectric liquid, which viscosity is just few times higher than that of water. The inner cylinder is heated and the outer one is cooled.

When a dielectric fluid in an annulus is under common action of a radial temperature gradient and a radial alternating electric field, the variation of dielectric permittivity with temperature creates a radial stratification of the permittivity. This stratification, and the radial inhomogeneity of the electrical field, leads to the generation of a radial electric buoyancy force, which increases with increasing the applied high tension and/or with decreasing the annulus radii. An outstanding effect of this electric buoyancy force is an enhancement of heat transfer thanks to the convective flow pattern it creates Chandra and Smylie (1972), Takashima (1980), Smieszek et al. (2008).

However fundamental properties of the electro-hydrodynamic instabilities for cylindrical annulus have to be clarified, and further aspects arise due to the competition with natural convection. In Fig. 1 two cases of radial temperature gradient

induced convection are distinguished. On the left side, the flow formation is resulting from natural gravity  $g$ , which is present in a laboratory. On the right side, a radial gravity  $g_E$  is set-up in micro-gravity  $\mu g$  conditions by means of an electric field, which will be discussed afterwards. The set-up in a natural gravitational buoyancy field leads to a fluid movement in form of a single convective cell, in which hot fluid is rising at the inner heated boundary and cold fluid is sinking at the outer cooled boundary. The top and bottom part of the system shows horizontal movement, again in boundary layers. The strengthening of temperature gradient results into instabilities of that convective motion, as presented by means of a stability analysis and direct numerical simulation in Mutabazi and Bahloul (2002). The instabilities are characterized by small scaled convective cells, which start to develop in the center of the annulus.

The set-up of a pure radial gravity leads to much more complex patterns. An initial experimental and numerical study on the stability of thermal convection in such dielectric-insulating fluids were done by Chandra and Smylie (1972). They conclude, that it is feasible to overlay the axial natural gravity with a radial gravity, due to a high voltage field, and observed the onset of thermal convection with temperature and power measurement of the heat transfer. Takashima (1980) extended the work of Chandra and Smylie and solved numerically the linear stability problem. In both numerical studies, the flow system was considered to be infinite. However, the impact of the electrical field on the flow has not been fully clarified.

To filter out the pure electro-hydrodynamic effects, reduced gravity conditions are required. Parabolic flights give that opportunity, to investigate thermal convection and heat transfer in three different gravity conditions, see Fig. 2. Additionally to

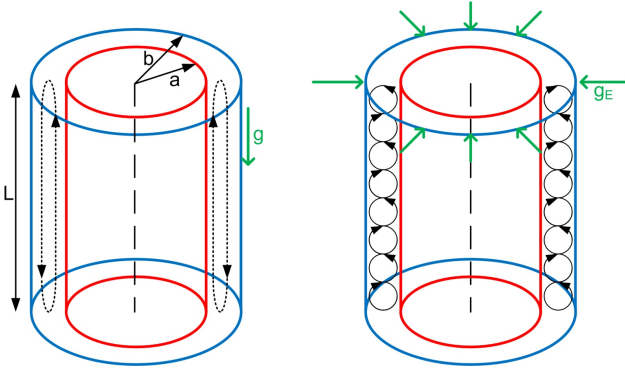


**Fig. 1:** Schematic representation of the annular cavity with natural axial gravity  $g$  as first case and with radial gravity  $g_E$  as second case. The expected convective cell formation is plotted.

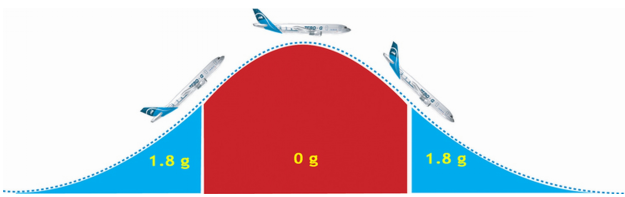


**Fig. 2:** Natural gravity ranges in one parabola of a parabolic flight. Each parabolic flight consists of 31 parabolas. Image source: Novespace.

the 1g-laboratory situation, there are hyper-gravity ranges with an approximately double- $g$  axial force field, i.e. 1.8 $g$  for about 20 seconds, and the micro-gravity  $\mu g$  range, which is very close to zero- $g$  for a time-scale of 22 seconds.

With the goal to qualify that impact, Sitte and Rath (2003) set up an electrode experiment and, moreover Sitte et al. (2001) and Sitte Sitte (2004) performed a first parabolic flight experiment, in which they used a Schlieren-technique for fluid flow monitoring in the azimuthal plane, and only during the  $\mu g$  phase. In addition, their electrode experiment implicates the application of the dielectrophoretic force as flow control parameter in thermal convective effects, by controlling the onset of instabilities, due to  $g$ , with superposition of radial buoyancy, due to  $g_E$ .

This work will present thermal convection experiments in the vertical annulus for both buoyancy forces, the axial and the radial gravity. First it will introduce the physical basics, followed by the description of the experiment setup. Afterwards, the presentation of first results, which refer to three different situations; first the natural convection in the axial gravity, second the thermal convection in the radial gravity, and finally, the superposition of both gravities.

## 2. Physical basics

### 2.1. Thermal electro-hydrodynamic convection

The hydrodynamic convection in fluids, which are caused by density and temperature gradients, are described with the equations of continuity, motion and heat conduction. Before

introducing these equations for the system, the analogy of temperature induced density changes and temperature induced permittivity changes will be discussed, which supply a so called thermal electro-hydrodynamic convection.

Regarding temperature gradients in incompressible and iso-viscous homogeneous Newtonian fluids, with low values for the coefficient of volume expansion  $\alpha$ , it is possible to assume a linear dependency for density changes, with the functional relation for density  $\rho$  and temperature  $T$ , Chandrasekhar (1981) describe:

$$\rho = \rho_0[1 - \alpha(T - T_0)], \quad (1)$$

with  $\rho_0 = \rho(T_0)$ ,

where the index  $_0$  marks the reference values for the used variables. This is known as the Boussinesq approximation, which also sets the density  $\rho$  as constant in all terms of the conservation laws, besides the external force, i.e. the buoyancy force itself.

In analogy to this buoyancy force, which is raised by density changes in natural gravity, there exists an electro-hydrodynamic buoyancy force, if the permittivity varies in dielectrophoretic force field:

$$\epsilon = \epsilon_1[1 - \gamma(T - T_0)], \quad (2)$$

with  $\epsilon_1 = \epsilon(T_0)$ .

Here, the temperature-dependency of the dielectric permittivity  $\epsilon$  is described with  $\gamma$  as the thermal expansion coefficient, relating also with the following:

$$\gamma = \alpha \frac{(\epsilon_r - 1)(\epsilon_r + 2)}{(3\epsilon_r)} \quad (3)$$

with  $\epsilon_r$  as the relative permittivity of the fluid, as shown by Yavorskaya et al. (1984). That dielectrophoretic force field is realized by means of an alternating high voltage potential between the inner and outer boundaries of the system and the use of a dielectric liquid as experimental fluid, as shown by Hart et al. (1986).

Considering the concentrically cylindrical set-up, the acceleration due to gravity is acting along the vertical axis, which refers to an axial force field. The acceleration due to the dielectrophoretic force is acting in radial acceleration due to the voltage potential set up between the inner and outer cylinder. This refers to a radial force field. While in the laboratory both forces superimpose each other, in micro-gravity environment the axial gravity tends to zero and offers the possibility to distinguish between both effects.

Refer to Yavorskaya et al. (1984), Hart et al. (1986) and also Futterer et al. (2010), who introduced this technique in spherical applications in long-term  $\mu$ -gravity experiments on space flights and on the International Space Station. Sitte and Rath (2003) introduced the technique for cylindrical application in short-term  $\mu$ -gravity conditions on parabolic flights.

### 2.2. Equations

The equations are scaled with outer radius  $b$  for length, the thermal diffusive time  $\tau_{therm} = d^2/\kappa$  for time, the temperature

difference  $\Delta T = T_a - T_b$  with  $T_a > T_b$  for temperature, where  $\kappa$  is the thermal diffusivity and the indexes  $a$  and  $b$  refer to inner and the outer base, respectively. The non-dimensional Boussinesq equations for velocity field  $\mathbf{U}$  and temperature field  $T$  for thermal convection under influence of a dielectrophoretic acting, radial buoyancy force field is described by the continuity equation:

$$\nabla \cdot \mathbf{U} = 0, \quad (4)$$

and by the Navier-Stokes-equation:

$$\rho \left[ \frac{\partial \mathbf{U}}{\partial t} + (\mathbf{U} \cdot \nabla) \mathbf{U} \right] = -\nabla p + \mu \nabla^2 \mathbf{U} + \rho(T)g + \epsilon(T)g_E \quad (5)$$

with the pressure  $p$  and the dynamic viscosity  $\mu$ . The gravitational acceleration is marked with  $g$  and the electro-hydrodynamical acceleration with  $g_E$ . The equation of energy conservation can be simplified to

$$\frac{\partial T}{\partial t} + (\mathbf{U} \cdot \nabla) T = \kappa \nabla^2 T \quad (6)$$

by neglecting the viscous and electric dissipation terms.

### 2.3. Parameters

The flow behavior depends on the physical properties for the fluid is described by the Prandtl number:

$$Pr = \frac{\nu}{\kappa} \quad (7)$$

with the kinematic viscosity  $\nu$ . The thermal buoyancy forces are balanced with the Rayleigh number. In natural buoyancy condition with axial gravity, the Rayleigh-number is defined to

$$Ra = \frac{\alpha g \Delta T (b - a)^3}{\nu \kappa} \quad (8)$$

with natural gravity  $g = 9.81 \text{ m/s}^2$  in axial direction, but it is only of relevance in the laboratory. The radial gravity is involved with the electrical Rayleigh number  $Ra_E$ :

$$Ra_E = \frac{\gamma g_E \Delta T (b - a)^3}{\nu \kappa} \quad (9)$$

with the radial acceleration  $g_E$ :

$$g_E = \frac{\epsilon_0 \epsilon_r}{\rho(T)} \frac{1}{2} \left( \frac{V_{app}}{\ln(a/b)} \right)^2 \frac{1}{b^3}, \quad (10)$$

which is induced by an alternating electrical field with the applied voltage  $V_{app}$  as peak-to-peak value.

### 3. Experiment setup

The experiment consists of two experiment cells. Each cell is a stationary coaxial cylinder system, see Fig. 1, with the radii  $a$  and  $b$  for the inner cylinder and for the outer cylinder respectively, and, in addition, the length  $L$  of the system. The cylindrical geometry is described with two non-dimensional parameters, i.e. the radius ratio  $\eta = a/b$  and the aspect ratio  $\Gamma = L/d$ .

**Tab. 1:** Geometrical parameter of the experiment. The experiment container contains two separate experiments with different radius ratio, presented with 'A' and 'B'.

Parameter		A	B
radius inner cylinder	$a[m]$	$5.0 \cdot 10^{-3}$	$4.7 \cdot 10^{-2}$
radius outer cylinder	$b[m]$	$1.0 \cdot 10^{-2}$	$5.2 \cdot 10^{-2}$
Length	$L[m]$	$1.0 \cdot 10^{-1}$	$1.0 \cdot 10^{-1}$
radius ratio	$\eta[ ]$	0.5	0.9
aspect ratio	$\Gamma[ ]$	$2.0 \cdot 10^1$	$2.0 \cdot 10^1$

**Tab. 2:** Fluid parameters of the working fluid Wacker AK5. The thermal expansion coefficient  $\gamma$ , applied in radial gravity in micro-gravity environment depends on the relative permittivity  $\epsilon_r$ , see Eq. 3.

Parameter		Value
kinematic viscosity	$\nu[m^2/s]$	$5.00 \cdot 10^{-6}$
density	$\rho[kg/m^3]$	$9.20 \cdot 10^2$
relative permittivity	$\epsilon_r[ ]$	2.70
therm. diffusivity	$\kappa[m^2/s]$	$7.74 \cdot 10^{-8}$
therm. expansion coeff.	$\alpha[1/K]$	$1.08 \cdot 10^{-3}$
therm. expansion coeff. for relative permittivity	$\gamma[1/K]$	$1.07 \cdot 10^{-3}$

Both experiment cells vary only in the radius ratio, aspect ratio and real scaled gap width  $d = b - a$  are equal. The geometric parameters are given in Table 1, too.

Besides the geometrical parameters, there are the fluid parameters of the used working fluid, i.e. silicone-oil Wacker AK5, which are summarized in Table 2. Finally the physical properties are captured with the Prandtl number of  $Pr = 64.64$ .

The thermal convection is realized by a temperature gradient between the heated inner and cooled outer cylinder. The fluid flow measurement is realized with tracer particles in the fluid and an axial laser light sheet illumination. Those particles are chosen in such a way, that they follow the fluid flow and, primarily, do not align in the applied high voltage potential.

The high voltage potential is connected to the outer cylinder made of glass. The inner surface of the glass tube is coated with Indium-Tin-Oxide *ITO* to have a conductive surface on the one hand. On the other hand, to have a transparent surface for observing the convective flow. The inner cylinder is made of aluminum and connected to ground. The functional principle is similar to a cylindrical capacitor.

A camera is installed perpendicular to the laser illuminated plane, see Fig. 3, and can observe the whole length of the investigation gap. Images are analyzed by cross-correlation functions, which is based on theories derived from a real particle image velocity (PIV).

The investigation distinguish between three buoyancy cases for the experiment. First, case introduce the natural convection in axial gravity. Second case regarding the set-up during a parabolic flight, i.e. the thermal convection in radial gravity.

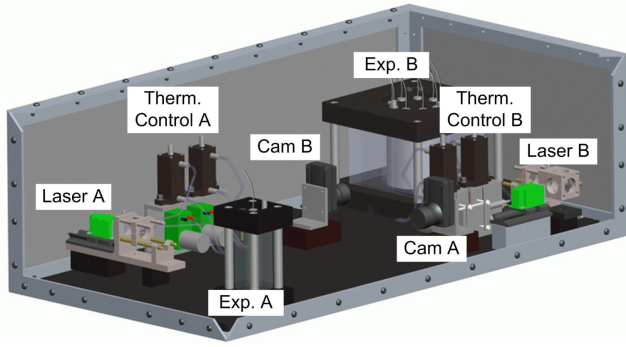


**Fig. 3:** Drawing for the fluid cell assemblies, integrated in the experiment container, including the measurement technique and thermal control. The fluid cell, which is marked with Exp. A has the smaller radius ratio  $\eta = 0.5$  and Exp. B with the  $\eta = 0.9$ , respectively.

And, third case will present the superposition of axial and radial gravity, inducing electro-hydrodynamic convection. For all the three cases, different approaches have been used. First, the  $\Delta T$  just increase and therefore the Rayleigh number  $Ra$ . During  $\mu g$  experiments the Rayleigh number  $Ra_E$  is varied, and therewith by keeping the thermal heating constant with  $\Delta T = 10K$  and the applied electrical field is varied with  $0kV \leq V_{app} \leq 10kV$ . In laboratory,  $\Delta T$  is varied between  $1 - 10K$  as well as  $V_{app}$  is varied between  $0 - 10kV$ , refer to Fig. 4 for illustration of the parameter domain. The  $Ra$ -axis characterize the variations in  $\Delta T$  and  $Ra_E$ -axis the variations in  $V_{app}$ , respectively. By varying buoyancy forces, there exist time scales, in which the pattern formation in the fluid is transient. The thermal diffusion time of  $\tau_{therm} = d^2/\kappa$  describes timescales, due to a variation of  $\Delta T$  and is  $\tau_{therm} \approx 5min - 40s$ . The viscous diffusion time  $\tau_{viscous} = d^2/\nu$  characterize the timescale of transient states in the fluid, due to the applied synthetic radial force field and is  $\tau_{viscous} \approx 5s$ .

The experiment container is integrated in an experiment rack, which is designed for installing in the aircraft for parabolic flights. The experiment can be controlled fully automatically, so as in parabolic flights with varying electrical gravity fields, as also in a laboratory with extended time scales.

## 4. Results

The following section presents the results for the three different convective set-ups, induced by axial natural and radial dielectrophoretic gravity in the laboratory and  $\mu g$ -environment, as describe in Fig. 4. In axial natural gravity  $g$ , the Rayleigh number  $Ra$  varies mainly with the temperature gradient  $\Delta T$ , as indicated on the x-axis in Fig. 4. The initial condition for the convective flow in radial buoyancy is fixed with  $\Delta T = 10K$  to the highest  $Ra$ . With the beginning of  $\mu g$ -environment the axial buoyancy tends to zero and the convective flow is driven only by the electrical Rayleigh number  $Ra_E$  due to strength of the applied high voltage field, as indicated on the y-axis in Fig. 4. In laboratory experiments natural and electrical gravity is superposed and therewith the parameter domain is captured in the region between.

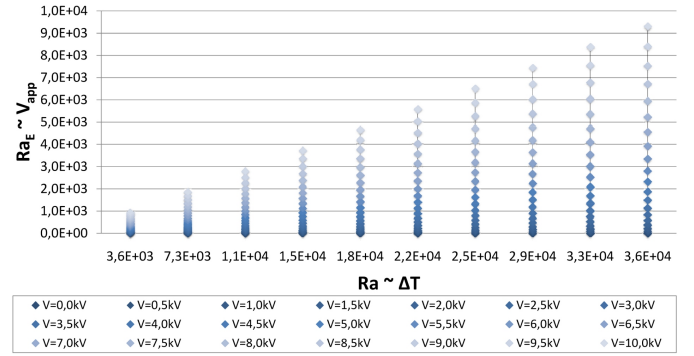


**Fig. 4:** Parameter domain of the experiment, where the  $\diamond$  marks the different set-points. The brightness of the  $\diamond$  increase with increasing high voltage field  $V$ . The variation of the axial buoyancy is characterized with  $Ra$ , which is adjusted on  $\Delta T$ , with  $1K \leq \Delta T \leq 10K$  in increments of  $1K$ . The variation of the radial buoyancy is described with  $Ra_E$  which is adjusted on the square of  $V_{app}$ , which is varied between  $0kV \leq V_{app} \leq 10kV$  in increments of  $0.5kV$ .

### 4.1. Axial buoyancy force field

For low Rayleigh numbers, which correlates with  $Ra \sim \Delta T$ , see Eq. 8,a single convective cell in the natural convection is expected, as shown in the left schematic in Fig. 1. For higher Rayleigh number it is expected, that the single convective cell is divided into several smaller cells, beginning in the center of the cylinder height, as shown by Mutabazi and Bahloul (2002).

The experimental setup is started at  $\Delta T = 2K$ , which corresponds to a Rayleigh number of  $Ra = 3.7 \cdot 10^3$  for both radius ratio. The observation starts after a waiting period of  $3 \cdot \tau_{therm}$  to ensure, that the flow is stabilized. The images in Fig. 5 visualize the velocity vector field from the PIV analysis algorithm, the axial and radial velocity component, as well as the vorticity. All components show very clearly the single convective cell, where the fluid rise upwards at the heated inner cylinder, which is always on the left boundary. At the cooled outer cylinder the fluid goes downwards, as expected. Moreover the top and bottom horizontal movement is visible, which are not captured by infinite cylinder systems in numerical simulation studies.

If  $Ra$  increases, by varying  $\Delta T$  in increments of  $1K$  to the maximum applicable temperature gradient of  $\Delta T = 10K$ . The Fig. 6 show, that the convective cells become unstable, with the wide gap  $\eta = 0.5$  more pronounced than the small gap with the radius ratio  $\eta = 0.9$ . But in both cases the single cell is not broken into smaller ones. This observation leads to the result, that the onset of first instabilities of the single convective cell is near.

### 4.2. Radial buoyancy force field

In this radial buoyancy force field, the focus is to investigate the transition to convective rolls in  $\mu g$ , coming from the single convective cell from the  $1g$  phase, which is stabilized in the  $2g$  phase due to the rise before the  $\mu g$  parabola, as shown in Fig. 2. In micro-gravity conditions, the effect of radial buoyancy without disturbances due to natural gravity can be observed. The natural gravity is reduced to a negligible mean gravity range of

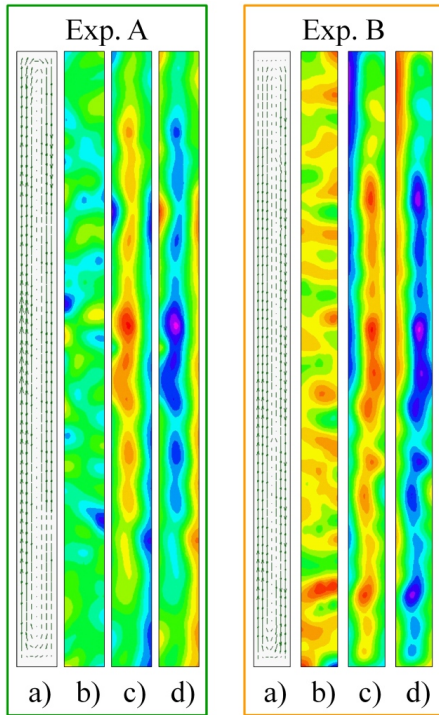


**Fig. 5:** Axial buoyancy at  $Ra = 3.7 \cdot 10^3$  for both radius ratios of  $\eta = 0.5$  in experiment A (left) and  $\eta = 0.9$  in experiment B (right). The frames show the mean of a) the vector field of the velocity, b) the axial velocity, c) the radial velocity and d) the vorticity of the flow. The radial temperature gradient in axial gravity fields delivers the single convective cell inside the annulus.

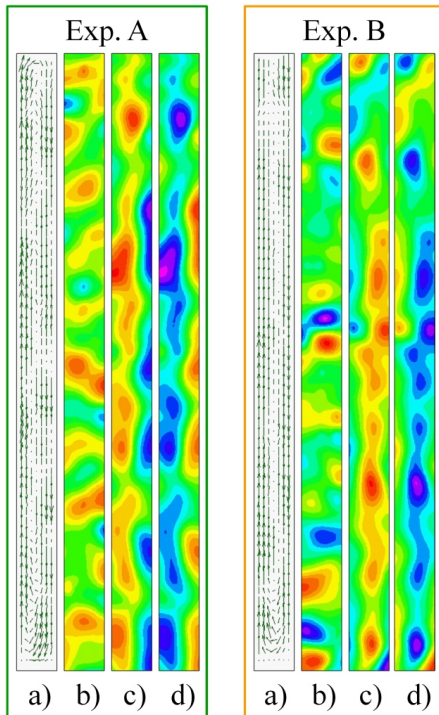


**Fig. 6:** Axial buoyancy at  $Ra = 3.6 \cdot 10^4$ , illustration follows that of Fig. 5. Transition into first instabilities of the single convective cell are visible for both radius ratio.

$\pm 0.05g$ , within the  $\mu g$ -range in parabolic flight. One parabolic flight includes 31 parabola, which is used to define the increment for  $Ra_E$  to  $\approx 610$ , the temperature gradient is fixed to  $\Delta T = 10K$ , the applied high voltage results from the set  $Ra_E$ ,  $\Delta T$  and the experiment parameter. Relating to the set-points of the experiment in Fig. 4, it means the last column with  $Ra = 3.6 \cdot 10^4$  was investigated during the  $\mu g$ -range in parabolic flight.

For a very low radial buoyancy, like in Fig. 7, the flow mostly 'freezes'. The vector in image part a) becomes very small, reduced to the size of a dot. For the greater radius ratio, this effect is more relevant, because for radial buoyancy force  $Ra_E \sim g_E$ , i.e. it relates with the square of the applied electrical field  $g_E \sim V_{app}^2$  and cubic of the geometry  $g_E \sim b^{-3}$ . This decreases the  $Ra_E$  for the experiment with  $\eta = 0.9$  enormously, and the impact of the radial buoyancy field, respectively. In the laboratory case (Sec. 4.1), the Rayleigh number  $Ra$  is equal for both radius ratio, it only depends on  $\Delta T$  due to constant  $g$ .

Other interesting aspect is observed. If the  $\mu g$  range starts and  $g$  vanishes, the thermal convection stops immediately. For small  $Ra_E$  there seems to be some kind of stratification effects with the tracer particles, with higher  $Ra_E$  this effect minimizes, as observable in Fig. 8, due to stronger movement of the convection. A similar effect can be observed in natural gravity condition with very small  $\Delta T$ , when the density of the particles and the fluid varies a bit. In radial gravity supervenes that little differences in permittivity between fluid and particles, lead to a similar effect, due to dielectrophoretic force. But these effects decrease with higher  $Ra_E$ , where is to be seen some kind of wavy movement in axial and radial direction for  $\eta = 0.5$  at the top part in the vector field of experiment A. In experiment B, the vector field shows a small increasing of movement along the centerline of the investigation gap. The velocity field in axial (b) and radial (c) direction confirm this identification in direct comparison of Fig. 7 and Fig. 8. The observation of the transition to more complex convective flow show promise to increase  $\mu g$  range to more than  $\tau_{therm}$  for more precise investigations, the more for small  $\eta$  than for big  $\eta$ .

#### 4.3. Superposition of axial and radial buoyancy force field

As already discussed in Sec. 4.1, a Rayleigh number of  $Ra = 3.6 \cdot 10^4$  (which means  $\Delta T = 10K$ ) is to low to break the stability of the thermal convective cell at these small scales. Now,  $Ra$  will be decreased to  $Ra = 7.3 \cdot 10^3$  ( $\Delta T = 2K$ ) and the radial buoyancy force field will be increased, by applying a radial electrical field, presented by the electrical Rayleigh number  $Ra_E$ .

With the superposition of axial and radial buoyancy force field an enhancement of heat transfer is observed in the numerical studies of Smieszek et al. (2008). By applying the electrohydrodynamic force field on a stable convective single cell, disturbances induce separations into convective cells, already at low temperature gradients.

First instabilities in the single convective cell are observed for the experiment with  $\eta = 0.5$ , as shown in Fig. 9. The experiment with  $\eta = 0.9$  show no response to the superposition

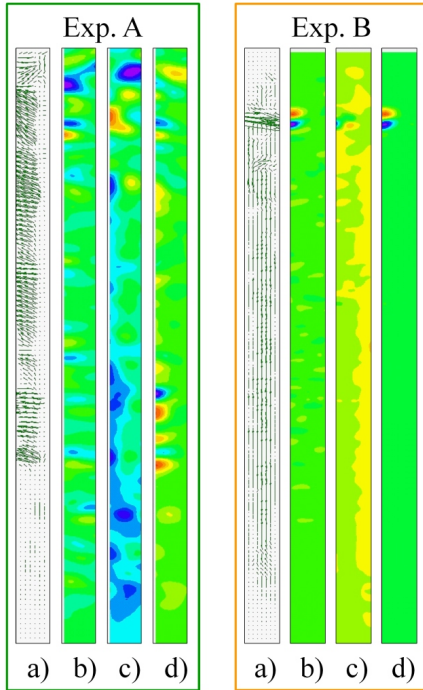


**Fig. 7:** Radial buoyancy at low  $Ra_E$ , illustration follows that of Fig. 5. Drift of particles in radial direction at  $Ra_E = 3.2 \cdot 10^2$  for experiment A with  $\eta = 0.5$ . For experiment B with  $\eta = 0.9$  the inertial convective cell is mostly frozen at  $Ra_E = 1.2 \cdot 10^2$ .

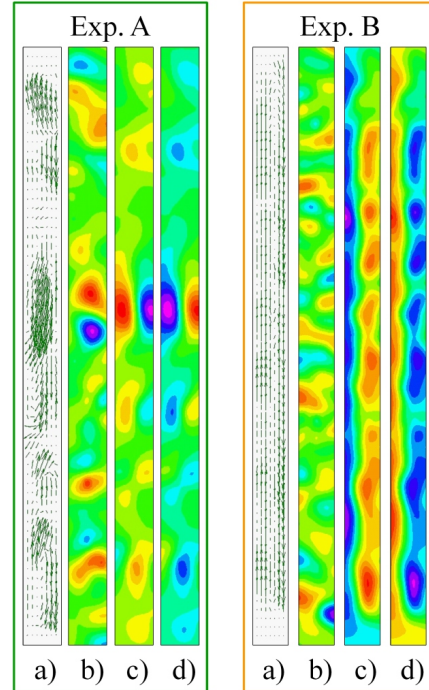


**Fig. 9:** Superposition of axial buoyancy with radial buoyancy at low  $Ra$ , illustration follows that of Fig. 5. The radial electrical field induce disturbances in the convective cell if there is a small radius ratio as in experiment A with  $\eta = 0.5$ .

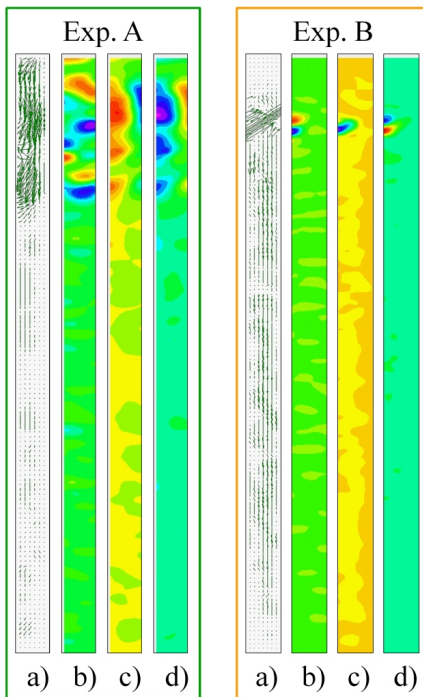


**Fig. 8:** Radial buoyancy at high  $Ra_E$ , illustration follows that of Fig. 5. Wavy movement of particles in radial and axial direction at  $Ra_E = 9.3 \cdot 10^3$  for experiment A with  $\eta = 0.5$  on top part of the cavity. Experiment B with  $\eta = 0.9$  show some concentration of particles along the centerline of the gap, the movement of particles is very low at  $Ra_E = 3.1 \cdot 10^3$ .

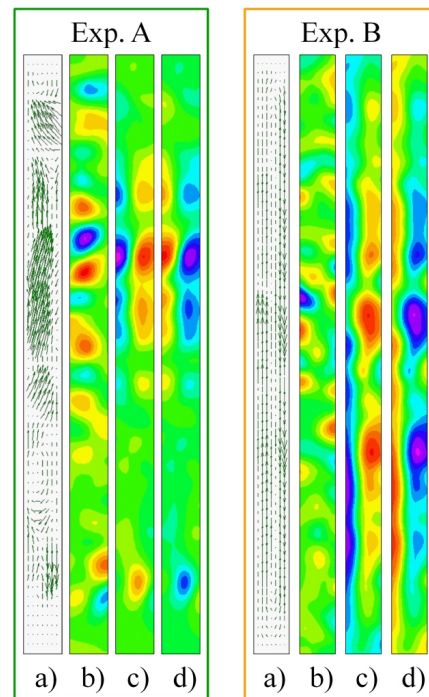


**Fig. 10:** Superposition of axial buoyancy with radial buoyancy at high  $Ra$ , illustration follows that of Fig. 5. In the annulus of large aspect ratio, there exists no single convective cell anymore. Instead of the small aspect ratio annulus in experiment B, where the radial buoyancy force field has no impact on the well known single convective cell.  $Ra_E$  is equal to Fig. 9 and  $Ra = 3.6 \cdot 10^4$ .

with the radial buoyancy field. The electrical Rayleigh number are  $Ra_E = 9.3 \cdot 10^3$  for experiment A and  $Ra_E = 3.1 \cdot 10^3$  for experiment B. The strength of the applied high voltage is  $V_{app} = 10kV$  for both  $Ra_E$

Also at high  $Ra = 3.6 \cdot 10^4$  ( $\Delta T = 10K$ ) is the effect of the radial buoyancy force field on the convective cell, due to the natural gravity, not observable for  $\eta = 0.9$ , see Fig. 10. For the radius ratio  $\eta = 0.5$  the effective superposition is increased, which become clear by comparing the axial (b) and the radial (c) velocity field of both experiment set points (Fig. 9 and Fig. 10).

These first results demonstrate that the application of electrical fields as additional buoyancy force field to the natural gravity lead to an enhancement of heat transfer. Further it is possible to control the thermal convection due to setting up the strength of the electrical field.

## 5. Outlook

The combination of a radial temperature gradient and an alternating electrical force field has great impact on fluid flow patterns, which organize the heat transfer on convection. The presented results demonstrate, that a convective motion in the homogeneous fluid can be controlled by the dielectrophoretic effect.

Further planned studies with a variation of the Prandtl number will help to analyze the onset of instabilities in detail. Moreover the system shall be analyzed with the focus on power measurement. This power measurement assigned to the Nusselt number will afford a quantitative analyzes of the enhancement of the heat transfer.

## Acknowledgments

The “Convection in Cylinders (CiC)” project is funded by the German Aerospace Center DLR within the “GeoFlow” project (grant no. 50 WM 0122 and 50 WM 0822). The authors would also like to thank ESA (grant no. AO-99-049) for funding “GeoFlow” and the “GeoFlow” Topical Team (grant no. 18950/05/NL/VJ). The scientists also thank the industry involved for support and parabolic flight, namely Novespace, Merignac, France and for providing fluids, namely Wacker AG, Munich, Germany. Furthermore fruitful discussions with Prof. Dr. Innocent Mutabazi and Dr. Olivier Crumerolle, CNRS-Université du Havre, Laboratoire Ondes et Milieux Complexes, Le Havre, France are gratefully acknowledged.

## References

- Chandra, B., Smylie, D. E., 1972. A laboratory model of thermal convection under a central force field. *Geophysical Fluid Dynamics* 3, 211–224.
- Chandrasekhar, S., 1981. *Hydrodynamic and Hydromagnetic Stability*. Dover Publications, New York.
- Futterer, B., Egbers, C., Dahley, N., Koch, S., Jehring, L., 2010. First identification of sub- and supercritical convection patterns from “GeoFlow”, the geophysical flow simulation experiment integrated in Fluid Science Laboratory. *Acta Astronautica* 66 (1-2), 193 – 200.

- Hart, J. E., Glatzmaier, G. A., Toomre, J., 1986. Space-laboratory and numerical simulations of thermal convection in a rotating hemispherical shell with radial gravity. *Journal of Fluid Mechanics* 173, 519–544.
- Mutabazi, I., Bahloul, A., 2002. Stability analysis of a vertical curved channel flow with a radial temperature gradient. *Theoretical and Computational Fluid Dynamics* 16, 79–90.
- Sitte, B., 2004. *Thermische Konvektion in Zentralkraftfeldern*. Ph.D. thesis, University of Bremen.
- Sitte, B., Immohr, J., Hinrichs, O., Maier, R., Egbers, C., Rath, H. J., 2001. Rayleigh-Bénard convection in dielectrophoretic force fields. In *12<sup>th</sup> International Couette-Taylor Workshop* Evanston, IL, USA.
- Sitte, B., Rath, H. J., 2003. Influence of the dielectrophoretic force on thermal convection. *Experiments in Fluids* 34, 24–27.
- Smieszek, M., Crumeyrolle, O., Mutabazi, I., Egbers, C., 2008. Numerical simulation of thermoconvective instabilities of a dielectric liquid in a cylindrical annulus. *59<sup>th</sup> International Astronautical Congress IAC-08-A2.2*.
- Takashima, M., 1980. Electrohydrodynamic instability in a dielectric fluid between two coaxial cylinders. *Quarterly Journal of Mechanics and Applied Mathematics* 33 (1), 93–103.
- Yavorskaya, I. M., Fomina, N. I., Belyaev, Y. N., 1984. A simulation of central-symmetry convection in microgravity conditions. *Acta Astronautica* 11 (3-4), 179–183.